CERTIFICATION BY ANALYSIS I and II

G. Olivares, J.F. Acosta, and V. Yadav
Computational Mechanics Laboratory
National Institute for Aviation Research, WSU
Wichita, KS 67260-0093

ABSTRACT

Physical testing is increasingly being replaced by numerical simulation models because it provides a more rapid and less expensive way to evaluate design concepts and design details. In the aerospace industry, crashworthiness numerical simulation methods are primarily used at the very end of the product development process. Often they are applied to confirm the reliability of an already existing design, or sometimes for further design improvements by means of optimization methods. There are a number of CAE (Computer Aided Engineering) tools that could be used for solving aircraft crashworthiness problems. These are best utilized by using a systems approach that uses a combination of CAE analyses, component tests, sled and/or full-scale tests.

The intent of this research is to provide an overview of numerical modeling practices so that FAA and industry can gain an understanding of the fundamental modeling methods, a feeling for the comparative usefulness of different modeling approaches, develop an appreciation of the modeling problem areas, and limitations of current numerical models.

1.0 INTRODUCTION

The research in CBA phase I was focused in developing methods to conduct certification by analysis of aircraft seats per Advisory Circular (AC) 20-146. Aircraft seating systems physical testing is increasingly being replaced by numerical simulation models because it provides a more rapid and less expensive way to evaluate design concepts. The principal goal of these modeling efforts is to use numerical models to accurately predict the results of physical tests. An accurate numerical model could potentially be used to evaluate the seating system in lieu of physical testing, saving both development time and cost. A means of establishing confidence in this predictive ability is needed. Towards that end, research has been conducted to provide the baseline test data required to define specifications for numerical occupant models of the Hybrid II and FAA Hybrid III anthropomorphic test dummies (ATD) suitable for aviation impact test simulations, provide procedures for validation of both multibody and finite element ATD models, and convey modeling design guidelines to assist modelers in developing efficient and accurate models. The data generated in this phase will provide the baseline data required to define Aerospace Recommended Practice (ARP) 5765. ARP 5765 will provide the specifications and performance criteria for aviation specific numerical ATD occupant models. It will define the minimum set of test parameters and data needed to evaluate the degree of correlation between the model and the physical test, and provide procedures for quantitative comparison of test and modeling results. A report summarizing all this work has been released[10.] Upon completion of the ATD databases validation process, the research was focused on the modeling of the seat structure. Results for the strain rate effects in the finite element modeling process of the

seat structure were presented last year. High strain levels are present in deformed crash components. Ignoring the strain hardening, and strain rate effects in numerical models may lead to an underestimation of the energy dissipated, and the structural performance of the aircraft seat. This year we have focused the research in the development of component test methods and validation procedures for the metallic components of the seat structure, seat belt webbing and seat cushion assemblies. Future work in CBA I will focused on the installation issues, such as row-to-row, bulkheads, etc.

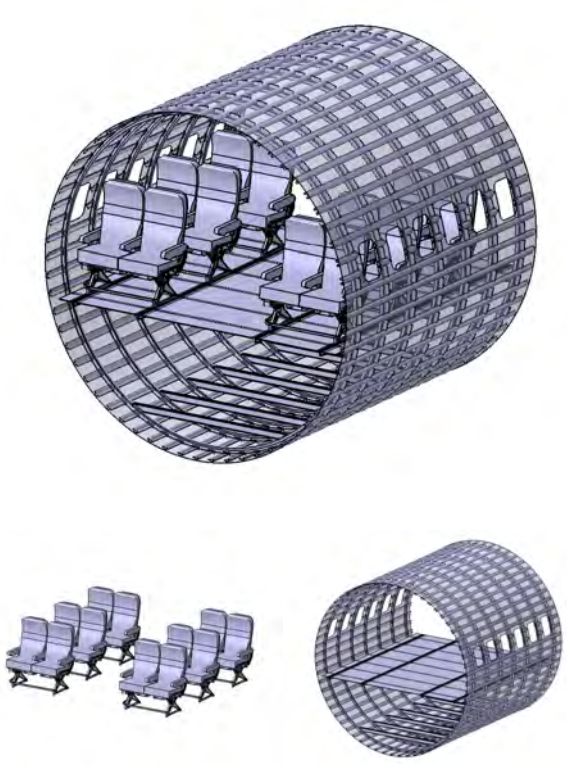

CBA I CBA II

Figure 1. CBA I and CBA II projects.

For the Certification by Analysis phase II, the work is focused in the crashworthiness performance of composite aircraft structures. Currently there are no

specific dynamic regulatory requirements for aircraft level crashworthiness. Nevertheless the FAA requires an assessment of each new design to ensure that the new aircraft design will not significantly depart from typical dynamic responses found in previous designs. Generally this assessment includes the evaluation of the survivable volume, retention of items of mass, deceleration loads experienced by the occupants, and occupant emergency egress paths. A significant amount of work on metallic aircraft structures has been conducted in the pass, but currently there is a lack of public domain data on the crashworthiness behavior of composite aircraft structures. The objective of this CBA phase II is to develop a numerical methodology for the design and certification of crashworthy composite structures. The work presented in this report summarizes the preliminary evaluation of composite material models at the coupon level. The current work presented in this paper summarizes the meso-scaled level approach.

2. MATERIAL CHARACTERIZATION SEAT BELT WEBBING

An experimental test protocol for obtaining the quasi-static stress-strain response of seat belt webbing over a predefined loading/unloading profile is described in this section. Figure 2 shows the specimen nominal dimensions along with the inclusion of tabs. The testing machine should have a stationary head (cross-head) and a movable head (actuator). The drive mechanism shall be capable of imparting the actuator a controlled rate of motion with respect to the cross-head. Standard servo-hydraulic systems are commonly used, see Figure 3. The test specimen shall be held between the actuator and the cross-head. Side loading wedge action grips are commonly used in tension testing of materials. Fixed type grips or self-aligning type grips can be used for that purpose. However, self-alignment grips are recommended. Hydraulic, pneumatic, or mechanical wedge grips rated for a minimum clamping pressure of 21 MPa (3,000 psi) shall be used for belt webbing testing. The material data is limited to the predefined loading pattern, see Figure 4. The loading/unloading profile should be defined with two different subsequent segments. In the first segment the test specimen should be loaded at a constant displacement rate up until a maximum load of 11,565 N (2,600 lbs). Then, without interruption the specimen should be unloaded back to the stating position at exactly equal displacement rate.

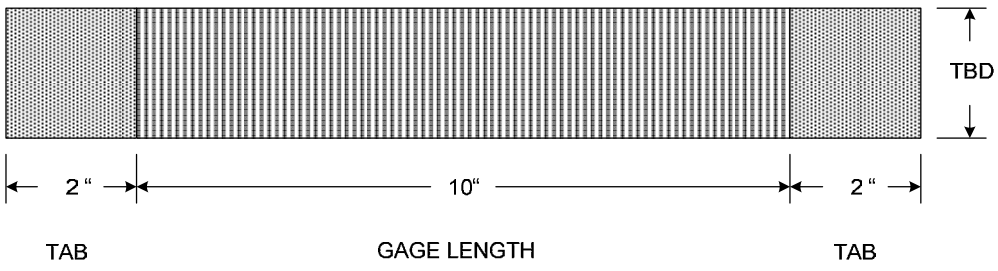

Figure 2. Test specimen with tabs.

The stress-strain response is intended as input data in material models used in numerical simulations of restrain systems at a component level and simulations where belt webbing is used as the restraint system. The tensile test method is design to meet the minimum tensile loads to demonstrate compliance according to Part 23.562 and Part 25.562 emergency landing dynamic conditions[1,2].

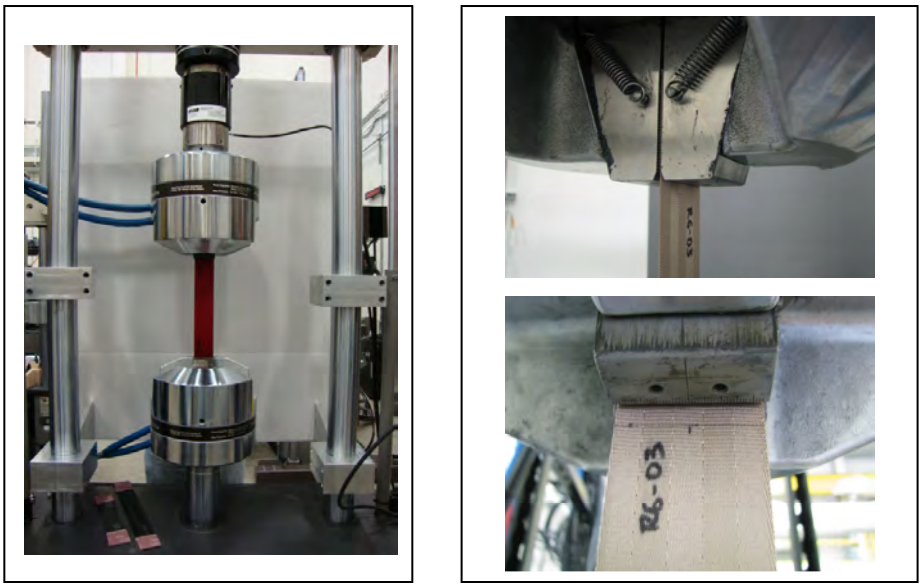

Figure 3. Test set-up and gripping wedges.

The test method is designed to obtain the static elongation limit of seat belt webbing over a predefined loading/unloading profile. The static elongation limit is calculated as the relative separation between grips obtained at the predefined maximum load. It shall be expressed as a percentage of the initial gage length of the test specimen. The static elongation limit of the seat belt shall be calculated at the maximum load observed by the belt webbing during the loading portion of the loading/unloading profile. At the same time static elongation graphs can be generated. The static elongation graph describes the seat belt webbing relative elongation with the applied force. It shall be generated including the loading portion and the unloading portion of the

predefined profile. Refer to Figure 4 for characteristic static elongation graphs for seat belt webbing indicating the extraction of the static elongation limit.

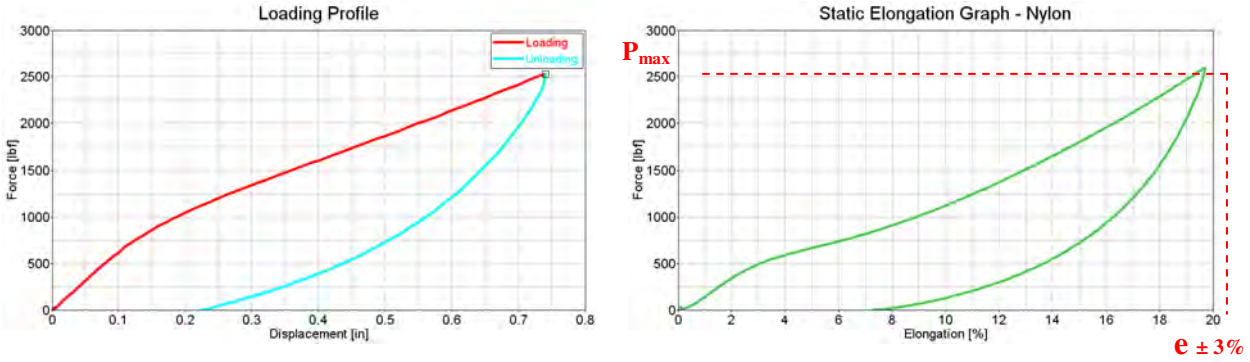

Figure 4. Test loading profile and typical static elongation graph for nylon.

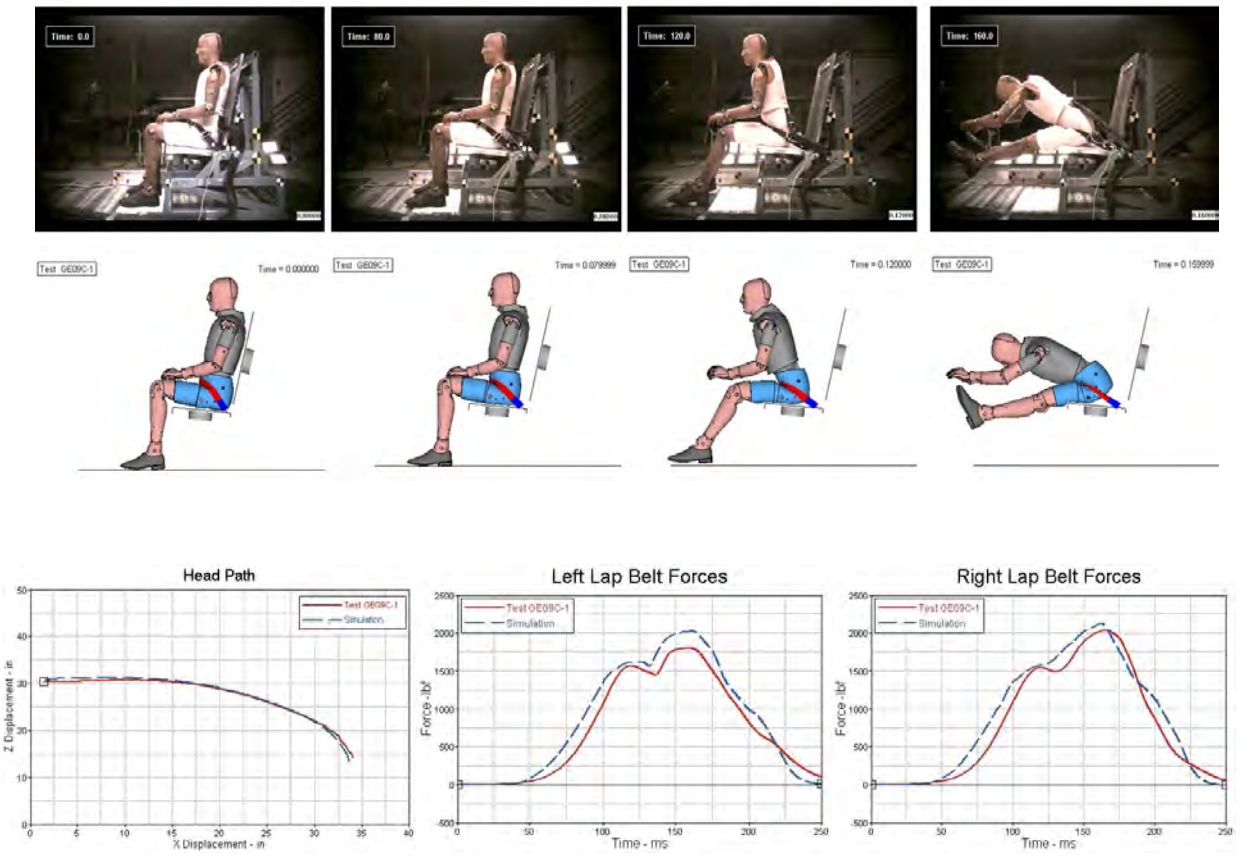

Figure 5. Example dynamic validation belt material model.

3. MATERIAL CHARACTERIZATION SEAT CUSHION

The test procedure is based on report number DOT/FAA/AR-05/5,I Development and Validation of an Aircraft Seat Cushion Component Test—Volume I[3]. The procedure is appropriate for typical upholstery and flotation foams used in the construction of aircraft seat bottom cushions. Test data obtained by following this test protocol is relevant for use in the component definition of seat cushions in numerical models. The test consists of compressing the test article under displacement control and recording the deflection and force applied during the experiment. The specimen is compressed at an actuator displacement rate of 0.762 m/s (30 in/sec) until a displacement equal to 90% of the specimen's original thickness is reached. At this point, the actuator releases the specimen at the same velocity as for the loading segment of the test and returns to its original position at the start of the test.

3.1 Test Apparatus

The test is performed using the high speed load frame and the fixtures available at the Mechanical Testing Laboratory at NIAR. The fixture consists of the perforated platen and indentor foot described in test B-1 of ASTM D3574[4]. The load frame has a capacity of 110 kip (489,000 N). It is equipped with a hydraulic actuator with a stroke of 0.254 m (10 in) and a capacity of 10 kip (44,000 N). The test is performed under displacement control at an actuator displacement rate of 0.762 m/s (30 in/s). The apparatus is equipped with a PCB 206 dynamic piezoresistive force sensor with a capability of up to 44,000 N (10,000 lb). The force data is to be collected at a rate of at least 10 KHz. The platen (horizontal plate support) is arranged to support the specimen on a level horizontal plate which is perforated with 0.00635 m (0.25 in) holes on

approximately 0.019 m (0.75 in) centers to allow for rapid escape of air during the test. Figure 6 shows the platen at NIAR. This platen was specifically designed for this type of test following the specifications on ASTM D3574 2. The indentor foot shall be a flat circular foot 8in in diameter self-aligning aluminum cap, which is placed over the MTS hemispherical platen to allow it to accommodate the angle of the sample.

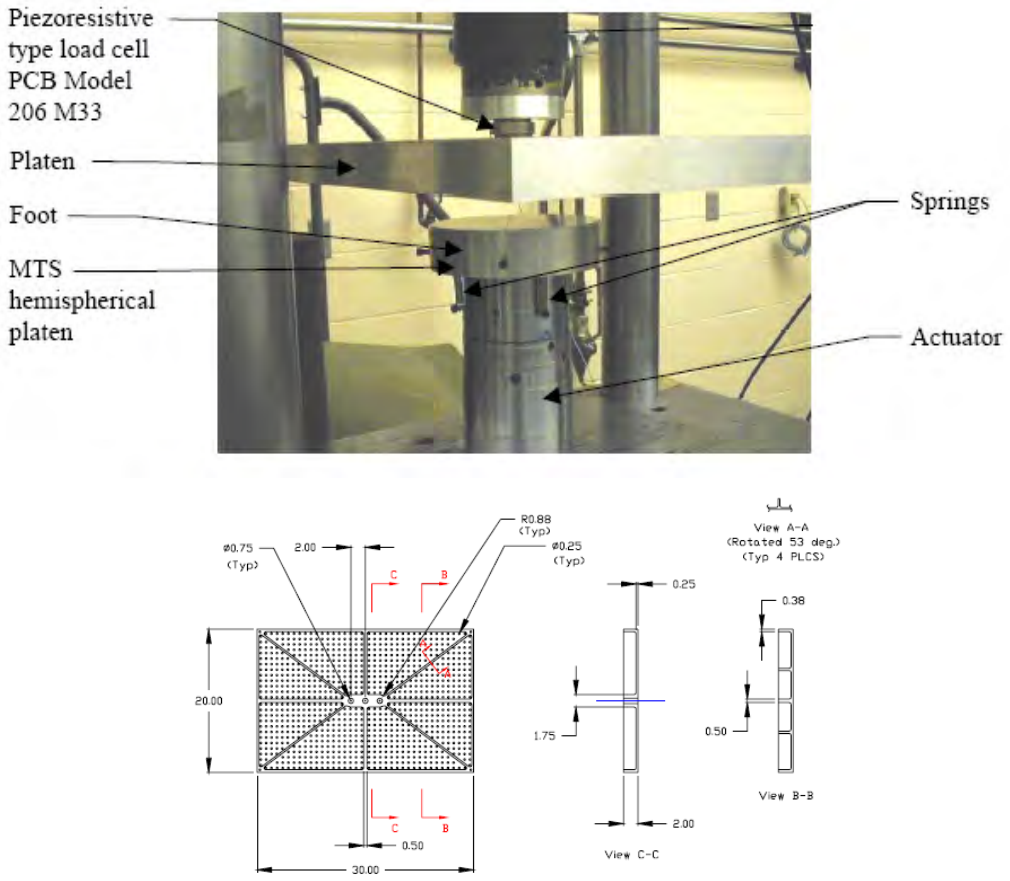

Figure 6. Test setup and platen description[3].

3.2 Test Article Description

The test article consists of a cylindrical sample of the foam used to construct the seat cushion. The specimen shall consist of a 0.19 m (7 1/2-in).-diameter cylinder. The upper and lower surfaces of the specimen are required to be parallel. The unloaded

specimen thickness shall represent the unloaded cushion thickness at the position of the anthropomorphic test dummy (ATD) ischial tuberosity (BRP) when the dummy is placed in the seat.

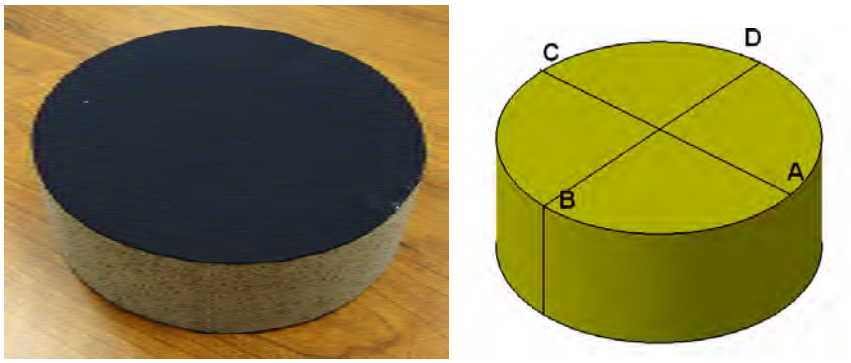

Figure 7. Typical cylindrical foam specimen.

3.3 Pre-Test Procedure

The specimens and fixtures shall be maintained at a temperature between 19º to 25ºC for a minimum of four (4) hours prior to and during the test. The cushions shall be maintained at a relative humidity of 10% to 70% for a minimum of four (4) hours prior to and during the test. All tests shall be performed seven (7) days or more after the foam has been manufactured. Pretest measurements must be taken and reported for each specimen, i.e., specimen thickness at points A through D as shown in the Figure 7.

3.4 Dynamic Test Procedure

Place the specimen flat and centered on the indentor foot. Raise the foot so that the specimen is in contact with the surface of the specimen. The specimen shall not be compressed. The loading of the specimen is divided into two segments:

- For the loading phase, the specimen shall be loaded in compression, under displacement control at a rate of 30 in/sec. The maximum deflection will

correspond to a ΔL/L of 0.9. For example: For a specimen that is 0.08 m thick, the actuator will be displaced 0.0072 m.

- For the unloading phase, the actuator will return to its original position at 0.762 m/s (30 in/sec).

Record the displacement of the actuator and the force measured by the load cell at 10,000 samples per second. Figure 8 shows an example of a typical specimen mounted on the test fixture and ready to be tested.

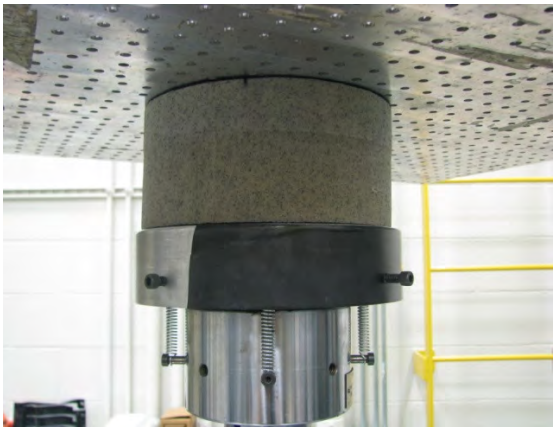

Figure 8. Typical set-up for dynamic testing of a foam specimen.

3.5 Validation Material Model – Component Level Tests

The main objective of this exercise is to obtain the dynamic force-deflection data for a rectangular seat cushion parting from the stress-strain characteristics (1-D data) of the foam obtained from the dynamic indentation force deflection test following the procedure described above. The force-deflection data obtained from samples of typical seat cushion foam is used to validate the procedure. A cylindrical specimen of DAX 55 foam of the specified diameter in the procedure and a nominal thickness of 0.15 m (6 in) is used to determine the material properties to be used in the simulation. Test data for a

cylindrical specimen and a square specimen can be seen in Figures 9 and 10 respectively.

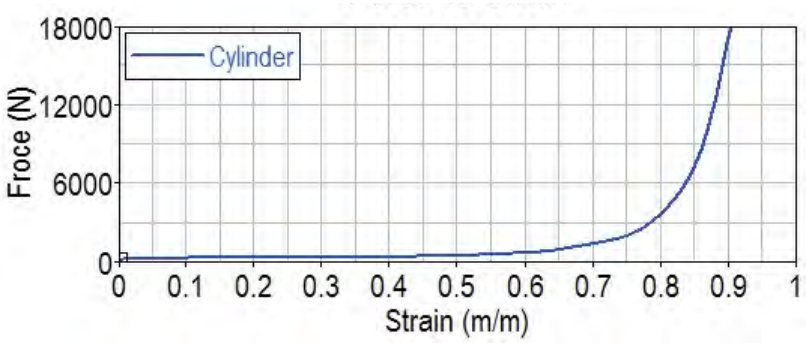

Figure 9. Force vs. strain curve of the cylindrical specimen.

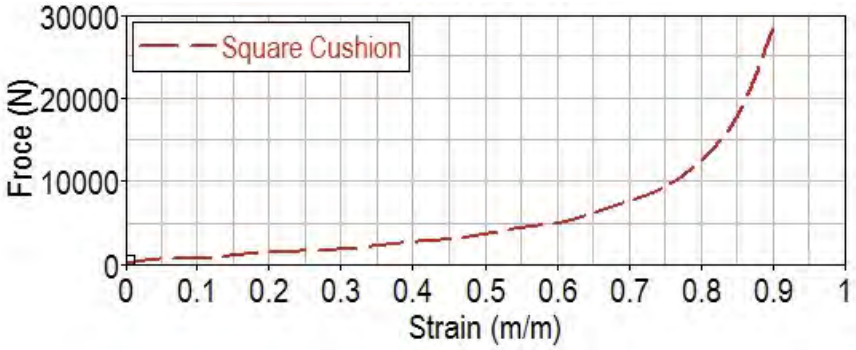

Figure 10. Force vs. strain curve of the square cushion.

3.5.1 Simulation Set-Up

A simulation is conducted using Ls-Dyna to evaluate the response of a square cushion subjected to the Force-Deflection test. In the simulation, the test fixture is modeled as a rigid part. The platen is attached to the bottom of the load cell through the *CONSTRAINED_EXTRA_NODE card and the top of the load cell constrained with the *BOUNDARY_SPC card. The force at the load cell was measured using the *DATABASE_CROSS-SECTION card.

The loading parameters set for the simulation are the same as for the component level test; the foot is set to displace at a rate of 0.762 m/s (30 in/s) a distance of 0.137 m (90% of the uncompressed cushion thickness). The Figure 11 shows an exploded view of the graphical representation of the numerical model.

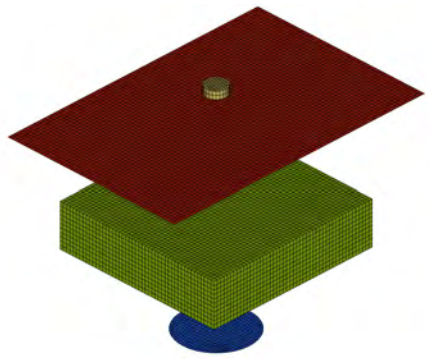

Figure 11. Exploded view of the numerical model.

The correct definition of the cushion material is critical to obtain good quality results from the simulation. The square cushion side length is approximately 0.5 m. The nominal thickness is equal to the cylindrical specimen. The foam is defined using the *LOW_DENSITY_FOAM material card available in LS-DYNA. The modulus of Elasticity E is obtained from the initial portion of the force-deflection curve. For the current example, only the loading portion of the stress-strain curve of the material is used to define the cushion since the unloading portion of the event is not critical for certification purposes. Therefore; HU = 1, BETA = 0 and SHAPE = 1. Tension cut-off 'TC' stress is left as the default value (1e20 MPa) since the cushion will not fail in tension in this example. Due to the large difference in stiffness between the cushion and the rigid parts of the model, the maximum allowed value of the viscous damping coefficient is used (0.5).

3.5.2 Simulation Results

A comparison between the experimental data of the cylindrical specimen and the square cushion is shown in Figure 12. The difference in the Force vs. Strain curves shows the effect that the boundary conditions have on the response of the cushion. Figure 13 compares the Force vs. Strain curve for the simulation of a square cushion with experimental results.

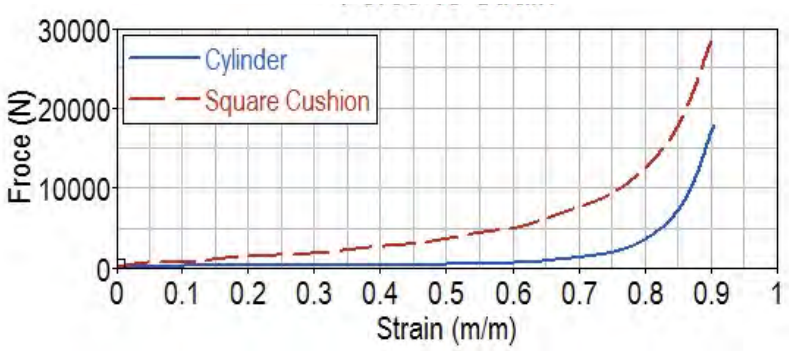

Figure 12. Force vs. Strain of the cylinder and the square cushion.

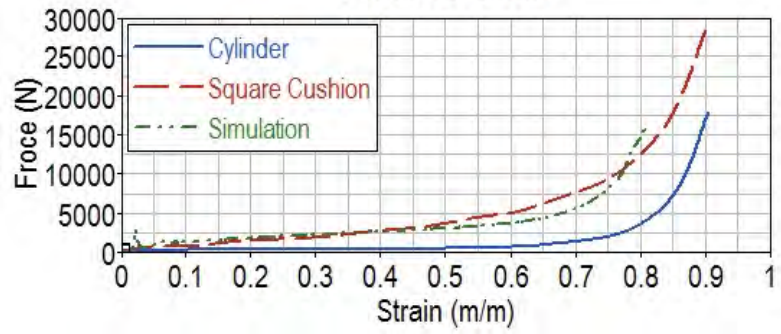

Figure 13. Force vs. Strain comparison.

The results of the component level simulation and the full scale dynamic seat test show that the defined test procedure is adequate to generate the material properties for typical aerospace seat cushions.

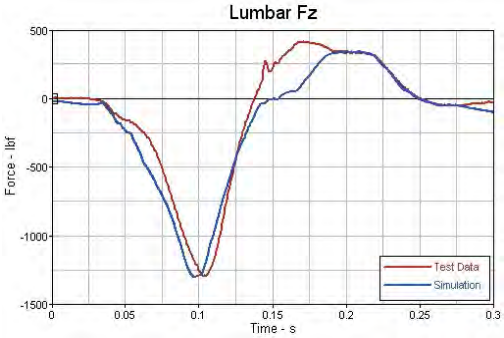

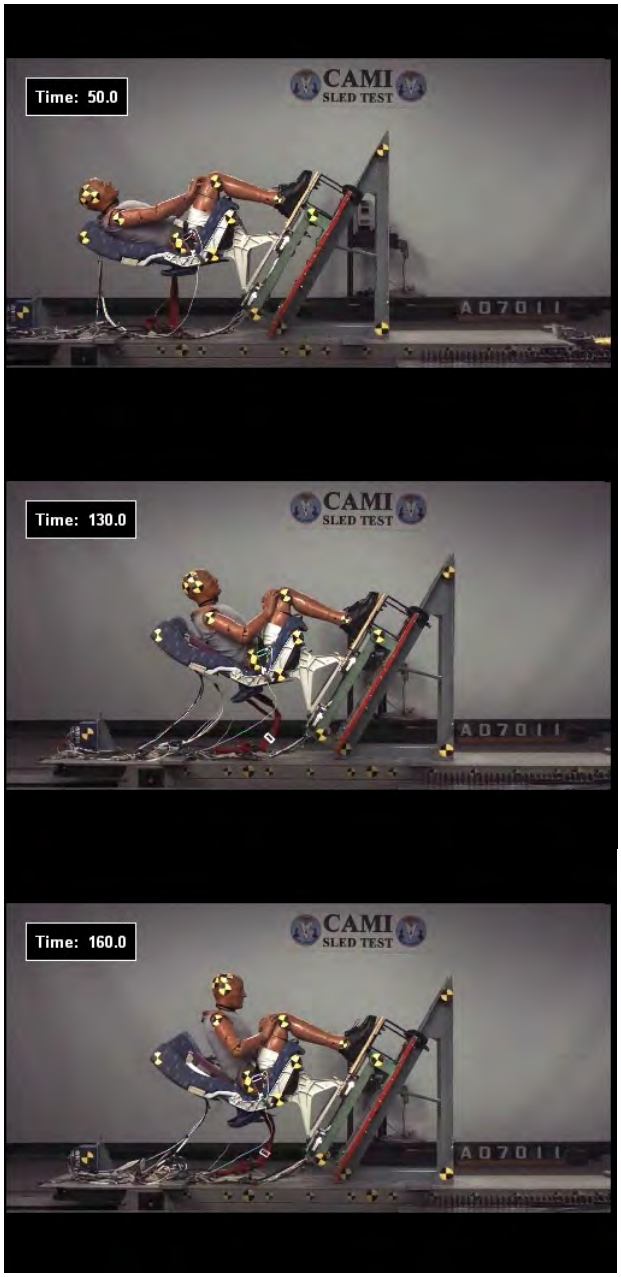

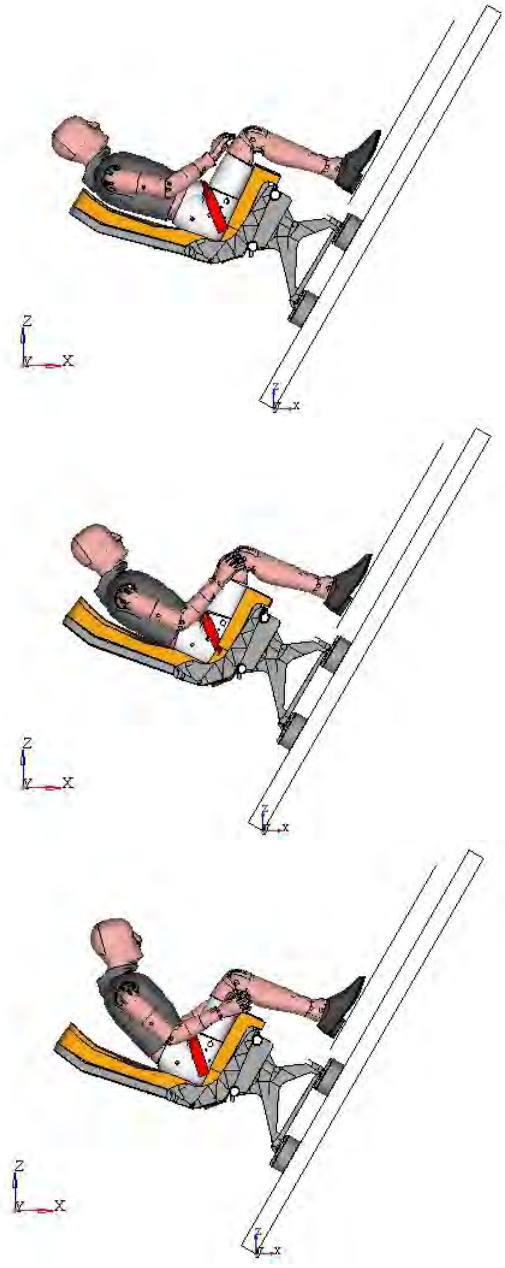

Figure 14. Lumbar load validation – Occupant kinematics.

4. METALLIC AND COMPOSITE MATERIAL CHARACTERIZATION

This section summarizes the high strain rate experimental and numerical evaluation of metallic and composite coupon level tests. The results and procedures for this section are used in both CBA I and II projects.

4.1 Material Systems

The materials for which experimental data is available from previous programs include aluminum 7075-T6 and three different Epoxy-Based composite material systems i.e., Newport E-Glass Fabric NB321/7781, Toray T800S/3900-2B Unitape, and Toray T700G-12K-PW/3900-2 (fabric). The aluminum specimen is a dog-bone type typical in tension testing in which a reduced cross section is desired to ensure failure in the gage section. Nominal dimension are presented in Figure 15. The specimen is design with an extended tab for accommodating a strain gage for load measurement, see Figure 5. The specimen is machined from a sheet of metal with common application in the aerospace industry. Laminated composite specimens for tensile testing are manufacture per ASTM D3039[5] but accommodating the geometry to high strain rate testing[6], see Figure 16. Stacking sequences included four different orientations, i.e., $[0]_N$, $[15/-15]_{NS}$, $[30/-30]_{2S}$, and $[45/-45]_{2S}$. However, the number of plies is limited for orientations $[0]_N$, $[15/-15]_{NS}$ to keep the load levels below the testing machine maximums.

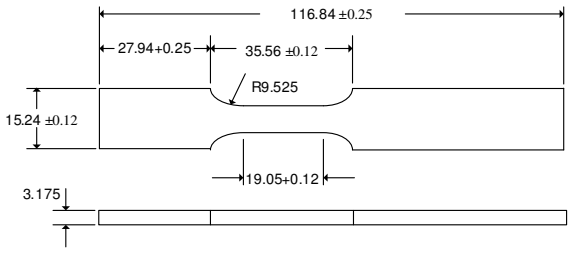

Figure 15. Benchmark tensile specimen geometry – Dimensions [mm].

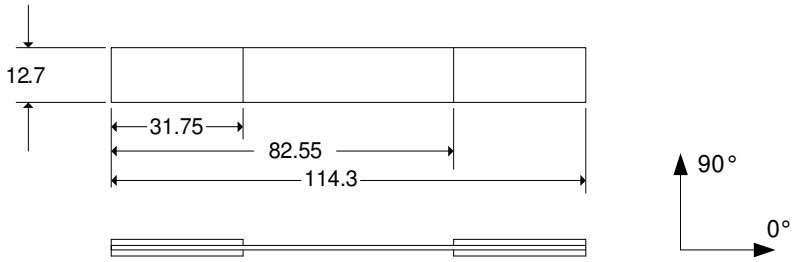

Figure 16. Tensile composite specimen geometry – Dimensions [mm].

4.2 Experimental Methods

Experimental data was available at various rates for each material system. However, for a fix stroke rate, the nominal strain-rate varied between the two specimen geometries as their gage length differs. The test matrix is presented in Table 1. Tests are conducted in a high stroke rate MTS servo hydraulic testing system rated for 22,241 N at rates as high as 12.7 m/s. Tensile testing grips are wedge grip assemblies designed for light weight at WSU, see Figure 17. The test set up includes a slack inducer mechanism designed to accelerate the actuator to the desired speed before the specimen is loaded[6]. Two methodologies are implemented for load measurement, i.e., a piezoelectric load cell and a strain gage mounted in the extended tab of the specimen as shown in Figure 18. The load cell is a PCB Piezotronics model 206M33 ICP calibrated for loads between 44,482 N and a frequency limit of 40 kHz.

Table 1. Test matrix – High strain-rate testing

MATERIAL / STACKING SEQUENCE	NOMINAL STROKE RATE [m/s]					
	0.000002	0.0025	0.025	0.253	1.269	2.538
$[0]_N$	x3	-	x3	x3	-	-
$[15/-15]_{NS}$	x3	-	x3	x3	-	-
$[30/-30]_{2S}$	x3	-	x3	x3	-	-
$[45/-45]_{2S}$	x3	-	x3	x3	-	-
AL-7075-T6	-	x3	x3	x3	x3	x3

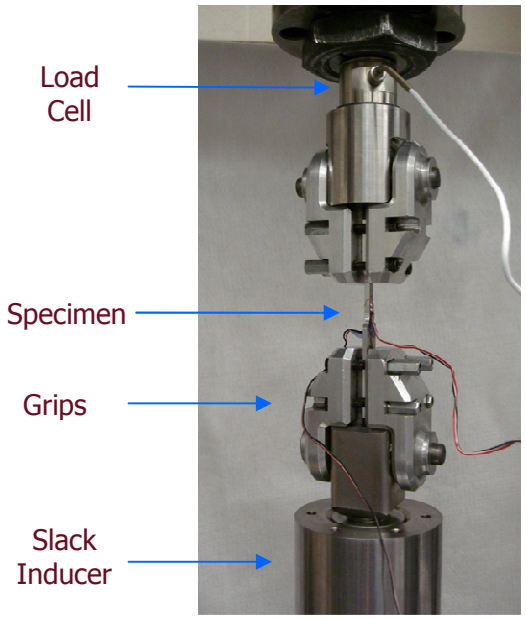

Figure 17. Tension grips at NIAR/WSU.

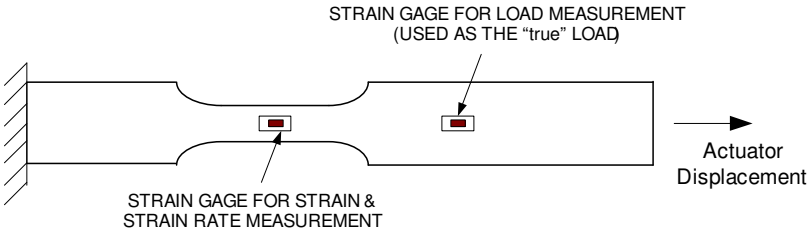

Figure 18. Strain gages location for load and strain measurement.

4.3 Experimental Data Evaluation

The variability in tensile high speed experimental data of Aluminum 7075-T6 and laminated composite materials is evaluated from quasi-static loading rates up to 2.54 m/s. The limitations of the testing technique and sources of variability are identified. Obtaining accurate experimental data suitable for material model generation represent the first challenge from experimental testing. Implementing finite element models as a predictable design tool requires accurate experimental data. Material properties along

with descriptive statistics for high speed tensile testing of Al-7075-T6 are summarized in Table 2 and in Table 3 for Newport E-Glass Fabric. The variability observed in the material properties is introduced by the testing technique and the measurement techniques. Conventional servo-hydraulic testing systems are used for low strain-rates (0.00167 - 10 s^{-1}) or high speed servo-hydraulic for strain-rates up to ~600 s^{-1}. No standard method or methodology to conduct high strain-rate testing is fully accepted up today. Secondary test devices necessary for load introduction as the test grips or devices for load transfer as pins and fasteners hinder the technique from introducing a constant strain rate. In addition, load measurement methodologies are affected by low natural frequency introducing ringing. Load cell data analysis contributes to the variability since there is not a standard procedure, i.e., various methods can be used as polynomial fitting, cut-off frequency method, or filtering or smoothing.

Additional limitations originate from the strain measurement technique. The stress-strain curves are limited by the specific operational range of the strain gages. Figure 19 exposes this problem. Notice the early failure of the strain gage in the strain history plot compared to the stress history plot. Such limitation truncates the stress-strain curve hindering the extraction of failure strength values from this curve. Conventional strain gages are limited to 5% and large deformation strain gages are limited to 20%. On the hand, other devices for strain measurement are still in a development stage.

Table 2. Summary of results for Aluminum 7075-T6

Stroke Rate [m/s]	Ultimate Stress [MPa]	Strain at Ultimate [mm/mm]	Young's Modulus [GPa]	Yield Stress [MPa]	Ave Strain Rate [s-1]
0.00254	522	0.08008	80.08	488.1	0.12
	577	0.04209	80.91	513.0	0.14
	544	0.10263	68.68	502.6	0.12
AVERAGE	**547**	**0.09136**	**76.56**	**501.24**	**0.13**
STANDARD DEVIATION	28	0.01595	6.8	12.47	0.01
CO-EFFICIENT OF VARIATION [%]	**5.06**	**17.45**	**8.93**	**2.49**	**9.12**
Stroke Rate [m/s]	**Ultimate Stress [MPa]**	**Strain at Ultimate [mm/mm]**	**Young's Modulus [GPa]**	**Yield Stress [MPa]**	**Ave Strain Rate [s-1]**
0.0254	615	0.11270	75.76	555.0	1.56
	590	0.09400	79.77	553.6	1.48
	575	0.19990	63.00	519.2	2.88
AVERAGE	**593**	**0.10335**	**72.84**	**542.59**	**1.97**
STANDARD DEVIATION	20	0.01322	8.8	20.29	0.79
CO-EFFICIENT OF VARIATION [%]	**3.45**	**12.79**	**12.02**	**3.74**	**39.84**
Stroke Rate [m/s]	**Ultimate Stress [MPa]**	**Strain at Ultimate [mm/mm]**	**Young's Modulus [GPa]**	**Yield Stress [MPa]**	**Ave Strain Rate [s-1]**
0.254	584	0.11770	81.97	525.4	12.18
	543	0.09140	48.97	493.7	10.76
	540	0.08180	71.81	470.2	10.64
AVERAGE	**555**	**0.09697**	**67.58**	**496.42**	**11.19**
STANDARD DEVIATION	25	0.01859	16.9	27.68	0.86
CO-EFFICIENT OF VARIATION [%]	**4.41**	**19.17**	**25.01**	**5.58**	**7.65**
Stroke Rate [m/s]	**Ultimate Stress [MPa]**	**Strain at Ultimate [mm/mm]**	**Young's Modulus [GPa]**	**Yield Stress [MPa]**	**Ave Strain Rate [s-1]**
1.27	528	0.10010	62.18	504.7	53.93
	661	0.11406	86.12	548.1	56.69
	539	0.01090	75.87	536.4	71.02
AVERAGE	**576**	**0.10708**	**74.72**	**529.74**	**60.55**
STANDARD DEVIATION	74	0.00987	12.0	22.47	9.17
CO-EFFICIENT OF VARIATION [%]	**12.80**	**9.22**	**16.08**	**4.24**	**15.15**
Stroke Rate [m/s]	**Ultimate Stress [MPa]**	**Strain at Ultimate [mm/mm]**	**Young's Modulus [GPa]**	**Yield Stress [MPa]**	**Ave Strain Rate [s-1]**
2.54	538	0.04805	65.12	518.5	155.6
	619	0.09365	72.15	530.2	105.2
	634	0.12148	76.42	549.5	111.56
AVERAGE	**597**	**0.10757**	**71.23**	**532.73**	**124.12**
STANDARD DEVIATION	51	0.01968	5.7	15.67	27.45
CO-EFFICIENT OF VARIATION [%]	**8.62**	**18.30**	**8.01**	**2.94**	**22.11**

Table 3. Summary of results for Newport E-glass $[0]_4$

Stroke Rate [m/s]	Ultimate Stress [MPa]	Strain at Ultimate [mm/mm]	Young's Modulus [GPa]	Ave Strain Rate [s-1]
0.00002	429	0.02778	19.51	0.000424
	437	0.02589	15.58	0.000389
	500	0.02847	15.65	0.000385
AVERAGE	**455.7**	**0.02738**	**16.91**	**0.000399**
STANDARD DEVIATION	38.9	0.00134	2.25	0.0000215
CO-EFFICIENT OF VARIATION [%]	**8.541**	**4.88**	**13.30**	**5.37**
Stroke Rate [m/s]	**Ultimate Stress [MPa]**	**Strain at Ultimate [mm/mm]**	**Young's Modulus [GPa]**	**Ave Strain Rate [s-1]**
0.0254	547	0.027124	29.82	0.3183
	585	0.029126	27.4	0.3226
	467	0.023218	23.41	0.3112
AVERAGE	**533.0**	**0.02649**	**26.88**	**0.317**
STANDARD DEVIATION	59.9	0.00300	3.2	0.006
CO-EFFICIENT OF VARIATION [%]	**11.239**	**11.34**	**12.04**	**1.81**
Stroke Rate [m/s]	**Ultimate Stress [MPa]**	**Strain at Ultimate [mm/mm]**	**Young's Modulus [GPa]**	**Ave Strain Rate [s-1]**
0.254	496	0.022656	39.20	1.9185
	610	0.031982	28.48	1.9939
	659	0.032373	24.65	1.9718
AVERAGE	**588**	**0.02900**	**30.78**	**1.96**
STANDARD DEVIATION	84	0.00550	7.54	0.04
CO-EFFICIENT OF VARIATION [%]	**14.22**	**18.97**	**24.51**	**1.98**

Figure 19. Stress-strain curve limited by strain gage capability.

4.4 Metal Material Model Definition

A piecewise linear plastic material model is implemented with Ls-Dyna MAT-24. It allows for the introduction of the effective stress vs. effective plastic strain to model the material response after the linear region and by this means it accounts also for rates effects. However, experimental data needs to be adjusted to represent the real material behavior, i.e., engineering stress vs. engineering strain should be converted to true stress vs. true strain. In the case of uniaxial tension, true stress vs. true plastic strain is equivalent to effective stress vs. effective plastic strain[7]. Figure 20 summarizes the three stress-strain curves.

A finite element model of the dog-bone specimen is assembled using Ls-Dyna. Dimensions represent the real testing specimen. Belytschko-Tsay shell elements with five (5) integration points are used to discretize the domain. Boundary condition and mesh are shown in Figure 21. The Top tab of the specimen is constrained not to move and a real displacement history is introduced to the bottom tab along *z* direction. Material properties are input into the material cards for each strain-rate validated.

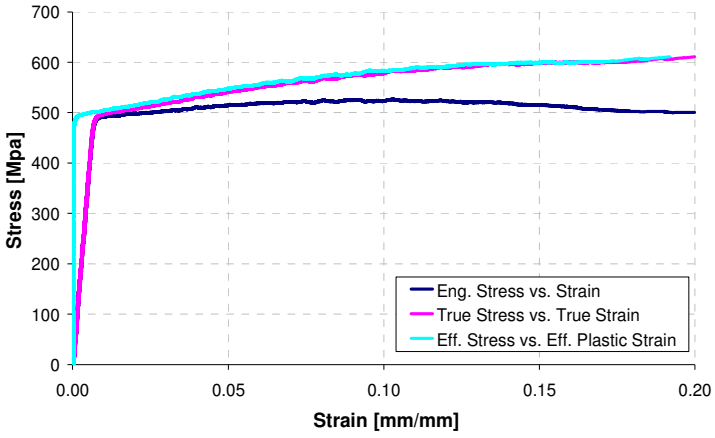

Figure 20. Stress-strain curves for Aluminum 7075-T6 - Strain-rate 0.133 s^{-1}.

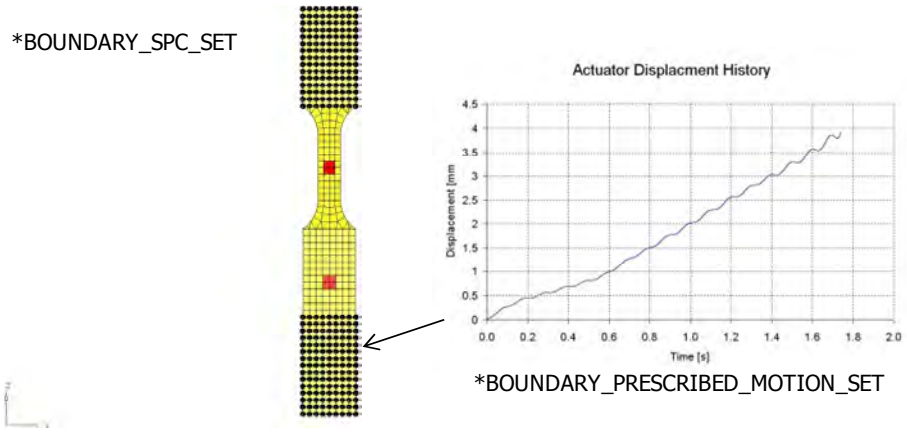

Figure 21. Specimen model boundary conditions.

4.5 Specimen-Gripping Assembly Model

A finite element model of the tension grips along with studs, pins, and the slack inducer mechanism is assembled to simulate the high speed servo-hydraulic testing system at NIAR/WSU, see Figure 22. The Aluminum experimental data is used to build a finite element model as a benchmark for high speed tensile testing simulation that can be extended to other materials testing and load cases. Several parameters that may interfere with high strain-rate testing can be evaluated, i.e., the effect of the grips masses, system compliance, etc.

The specimen for the specimen-gripping assembly model retains the same characteristics of the specimen model, i.e., dimensions, element formulation, and number of integration points. On the other hand, each part of the assembly is model with under-integrated constant stress solid elements. Material elastic was defined for those components that drive the systems compliance, i.e., pins and fasteners. The rest of the components were defined as rigid. Boundary condition and mesh are shown in Figure 23. The load cell at the top of the whole assembly is constrained not to move and

a real displacement history is introduced to the actuator along *z* direction. Material properties are input into the material cards for each strain-rate validated.

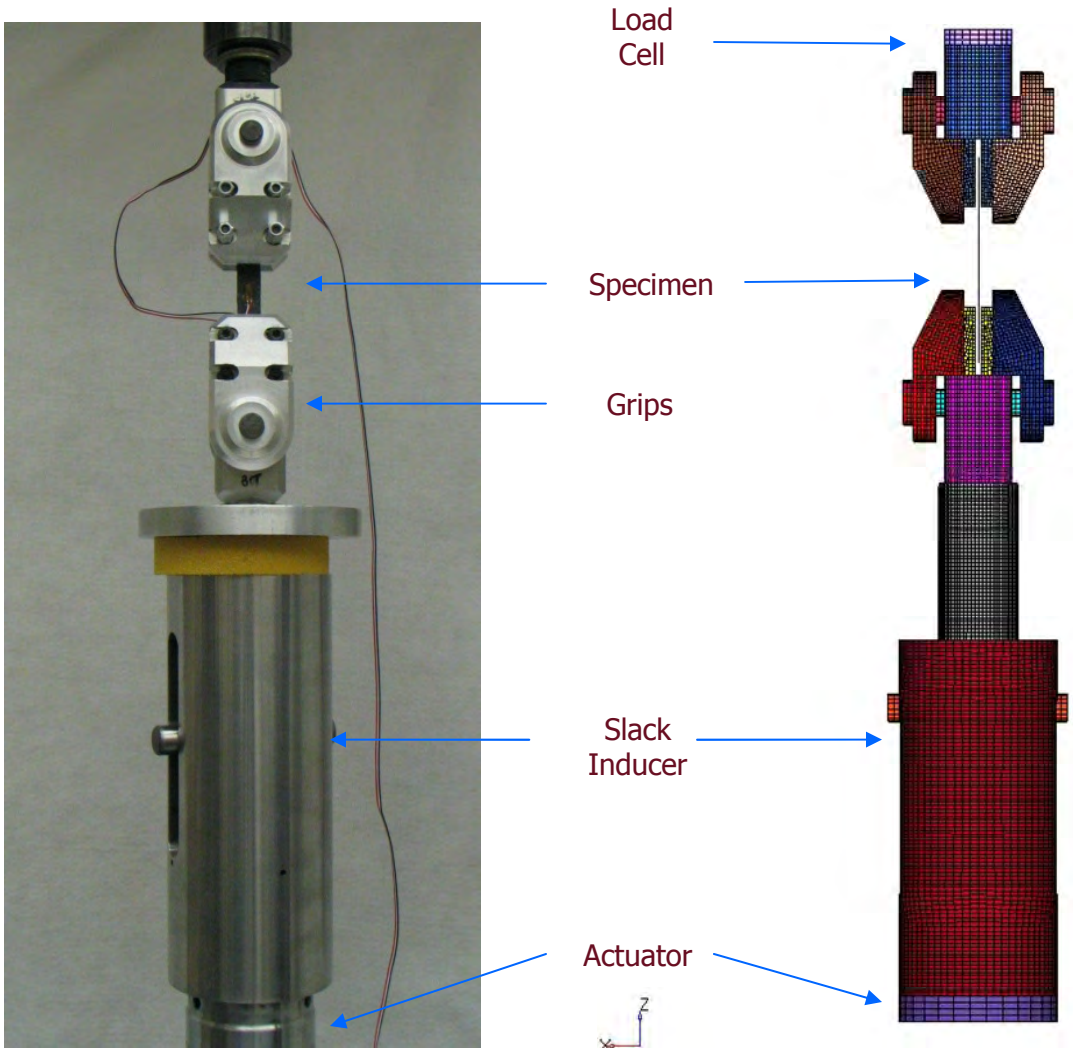

Figure 22. Specimen-Gripping assembly model of the high speed servo-hydraulic testing system.

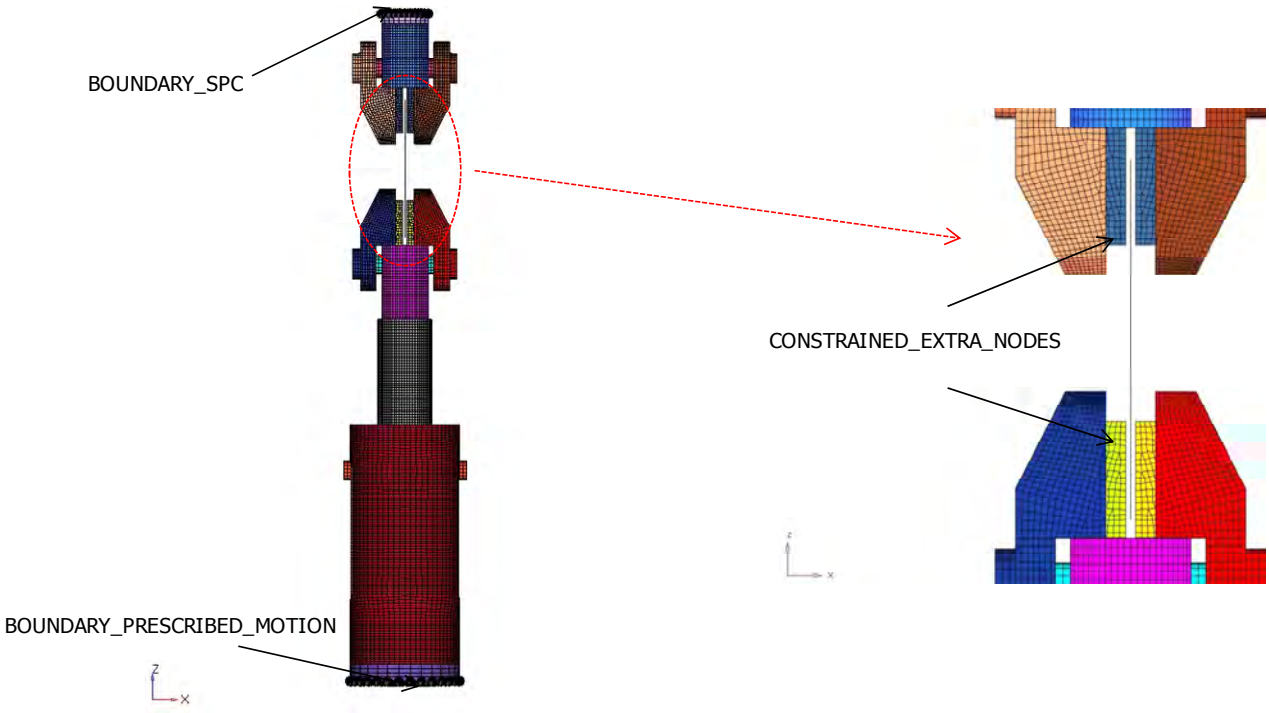

Figure 23. Assembly model boundary conditions.

4.6 Composite Material Model Definition

In general, three approaches can be taken to simulate composite materials depending on the level of detail required for the analysis[8], i.e., a micromechanics approach that consider the material at a constitutive level where fiber and matrix properties are defined along with their geometrical distribution, a meso-scale level approach where lamina elastic properties are defined along with layer thicknesses and fiber orientation, and a macro-scale level approach where laminate matrices [A], [B], [D], and [H] are defined but not stacking sequence, lamina properties or ply thickness. The current investigation follows the meso-scale level approach for which lamina properties where extracted from the experimental data available.

A material model for simulation of laminated composites is developed for tensile and compressive testing. Continuum mechanics models implemented in Ls-Dyna material cards MAT-54 and MAT-58 are used where composite materials are treated as linear elastic orthotropic before failure. The two material cards differ in the way pre-damage process and post failure process is handled. MAT-54 reduces fiber strength to account for matrix failure and implements a progressive failure model after yield. On the other hand, MAT-58 assumes deformation introduces micro cracks and cavities into the material causing stiffness degradation. Such reductions in the elastic module introduce nonlinearity to the deformation[9]. An example input for material cards MAT-54 and MAT-58 generated at a nominal strain-rate of 0.05 s^{-1} is shown in Table 4 and 5 respectively.

Table 4. MAT-54 input card Newport E-Glass $[0]_4$ – strain-rate 0.05 s^{-1}

Material ID	Density	EA	EB	EC	PRBA	PRCA	PRCB
	1.8E-09	24821	24821	500	0.138	77	0.0877

GAB	GBC	GCA	(KF)	AOPT			
4206	3447	3447		2			

			A1	A2	A3	MANGLE	
			0	1	0		

V1	V2	V3	D1	D2	D3	DFAILM	DFAILS
			0	0	0		

TFAIL	ALPH	SOFT	FBRT	YCFAC	DFAILT	DFAILC	EFS
0							

XC	XT	YC	YT	SC	CRIT	BETA	
540	547	540	540	137	54	0	

Taken from fabric results
Estimated
Agate

Table 5. MAT-58 input card Newport E-Glass $[0]_4$ – strain-rate 0.05 s^{-1}

Material ID	Density	EA	EB	EC	PRBA	TAU1	GAMMA1
	1.8E-09	24821	24821	500	0.138	91	0.0858
GAB	**GBC**	**GCA**	**SLIMT1**	**SLIMC1**	**SLIMT2**	**SLIMC2**	**SLIMS**
4206	3447	3447	0-1	0-1	0-1	0-1	0-1
AOPT	**TSIZE**	**ERODS**	**SOFT**	**FS**			
2		0-1	0-1	-1, 0, 1			
XP	**YP**	**ZP**	**A1**	**A2**	**A3**		
			0	1	0		
V1	**V2**	**V3**	**D1**	**D2**	**D3**	**BETA**	
			1	1	1		
E11C	**E11T**	**E22C**	**E22T**	**GMS**			
0.0256	0.0256	0.0256	0.0256	0.1822			
XC	**XT**	**YC**	**YT**	**SC**			
540	547	540	540	137			

Taken from fabric results
Estimated
Agate

A user-defined integration rule can be defined using Ls-Dyna card PART_COMPOSITE. It allows for the definition of element formulation, layer thickness, and material angle per integration point as seen in Table 6. The composite tension specimen is modeled with Belytschko-Tsay shell elements with as many integration points as layers. Dimensions represent the real testing specimen. Boundary condition and mesh is shown in Figure 24. The Top tab of the specimen is constrained not to move and a real displacement history is introduced to the bottom tab along *z* direction.

Table 6. PART_COMPOSITE input card for stacking sequence $[45/-45]_{2S}$

	1	2	3	4	5	6	7	8
1	PID	ELFORM	SHRF	NLOC	MAREA	HGID	ADPOPT	
		2	0.833	0.0				
2	FS	FD	DC	VC	OPTT	SFT	SSF	
3	MID1	THICK1	B1		MID2	THICK2	B2	
	6	0.27840	45		6	0.27840	-45	
4	MID3	THICK3	B3		MID4	THICK4	B4	
	6	0.27840	45		6	0.27840	-45	
5	MID5	THICK5	B5		MID6	THICK6	B6	
	6	0.27840	-45		6	0.27840	45	
6	MID8	THICK8	B8		MID8	THICK8	B8	
	6	0.27840	-45		6	0.27840	45	

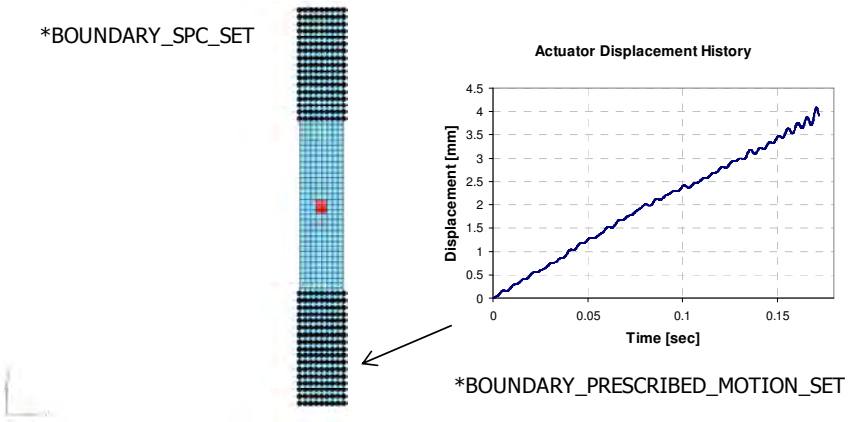

Figure 24. Composite tensile specimen model boundary conditions.

4.7 Analysis Results

4.7.1 Metal Material Model

The material model is validated with experimental data from quasi-static strain-rates to 133 s^{-1}. The average experimental stress-strain response for a nominal strain-rate of 133 s^{-1} is compared to the specimen simulation results in Figure 25. Good

correlation is observed. Hence, the stress-strain response of the material is captured over most of the duration of the test.

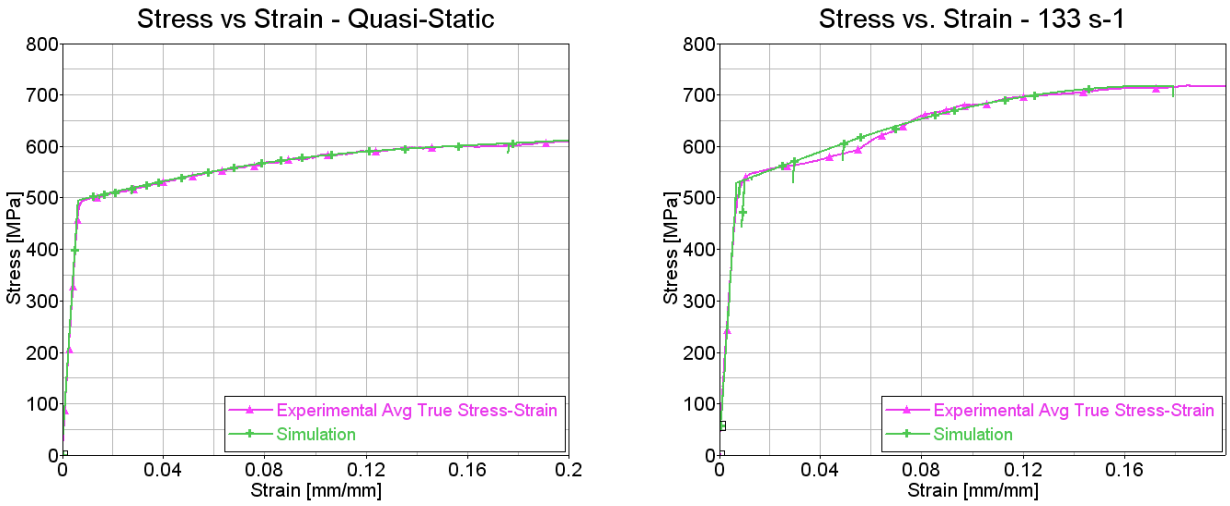

Figure 25. Al-7075-T6 Specimen model validation - Quasi-static and 133 s^{-1}.

4.7.2 Specimen-Gripping Assembly Model

The specimen-gripping assembly model is validated with experimental data ranging from quasi-static strain-rates to 133 s^{-1}. Simulation results at lower rates observed no deviation when compared to experimental data. Simulation results at higher rates observe some deviation in the individual response histories. However, the simulation stress-strain response fall closely to the experimental data, see Figure 26. In addition, the response for an artificial linear displacement input of 2.53 m/s is compared to the original experimental displacement input that only reaches 1.77 m/s. The plastic strain distribution is observed in Figure 27 and the failure mode in the simulation can be compared with the experimental results.

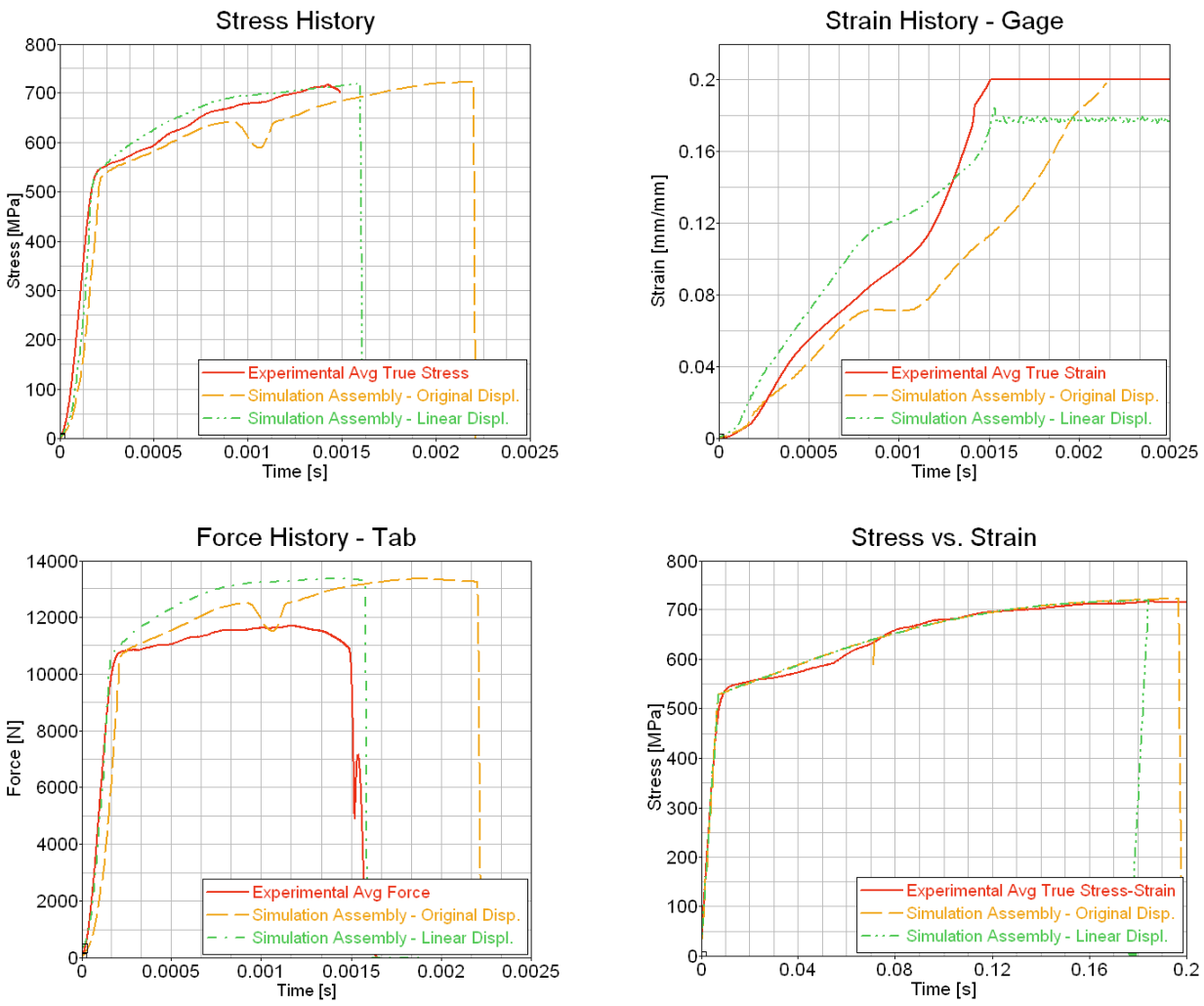

Figure 26. Specimen-Gripping model validation - strain-rate of 133 s^{-1}.

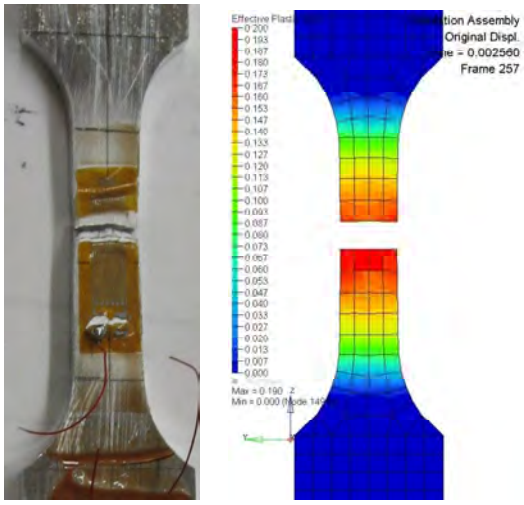

Figure 27. Effective plastic strain Al-7075-T6 - strain-rate 133 s^{-1}.

4.7.3 Composite Material Model

Newport E-Glass fabric 7781/NB321 tensile experimental data for various stacking sequences is used for evaluation and validation of the composite specimen model from quasi-static rates to 5 s^{-1}. Ls-Dyna material cards MAT-22, MAT-54, and MAT-58 are compared on Figure 28 and Figure 29 for two different material orientations at 0.5 s^{-1}.

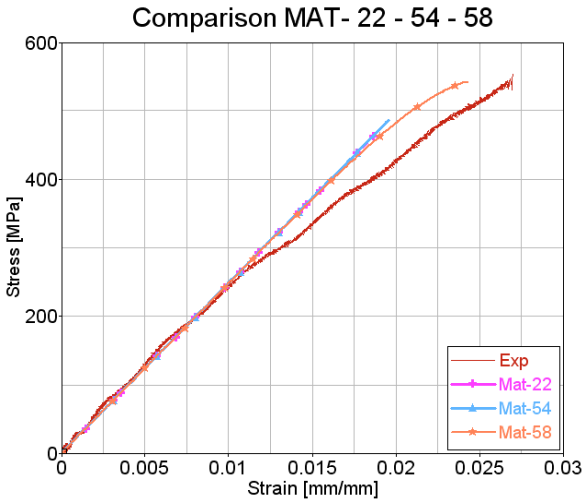

Figure 28. Composite specimen validation - $[0]_4$ strain-rate of 0.5 s^{-1}.

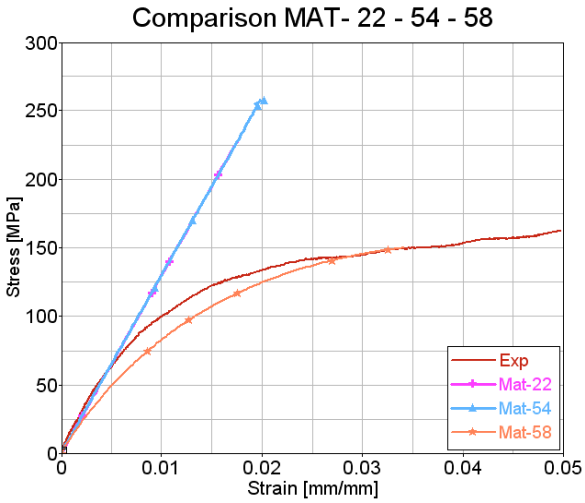

Figure 29. Composite specimen validation - $[45/-45]_{2S}$ strain-rate of 0.5 s^{-1}.

Material card MAT-58 seams to represent closely the non-linearity observed in the off-axis specimens without failure parameters manipulation. Thus, the material card is fixed and the different failure surfaces provided by the card are evaluated. Simulation results in Figure 30 and 31 seams to fall closely to the experimental data for failure surface FS=-1; faceted failure surface. The strain distribution is observed in Figure 32. The areas where larger strain values are observed clearly suggest the areas where failure can develop if compared with actual testing specimen.

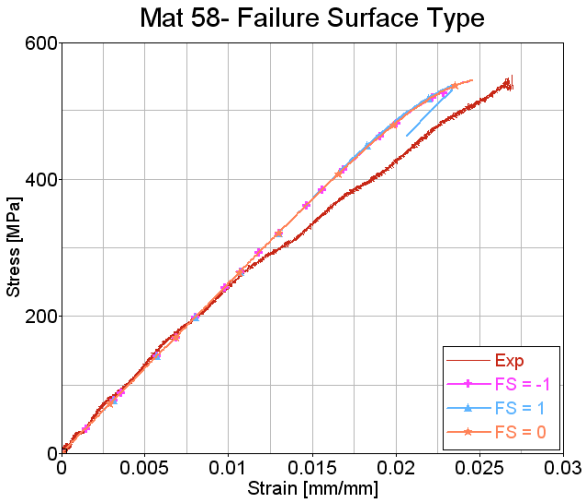

Figure 30. Failure surface comparison - $[0]_4$ strain-rate of 0.5 s^{-1}.

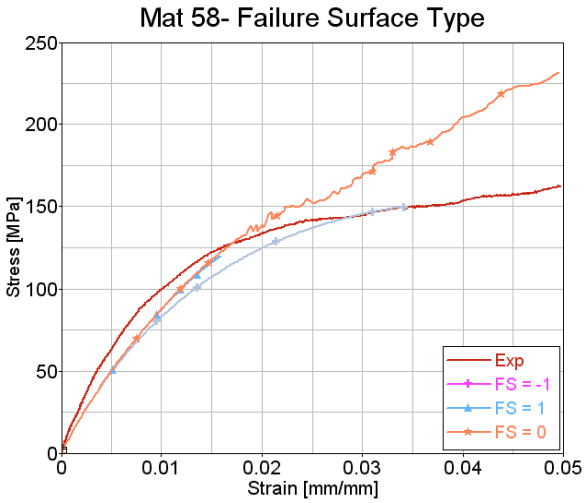

Figure 31. Failure surface comparison - $[45/-45]_{2S}$ strain-rate of 0.5 s^{-1}.

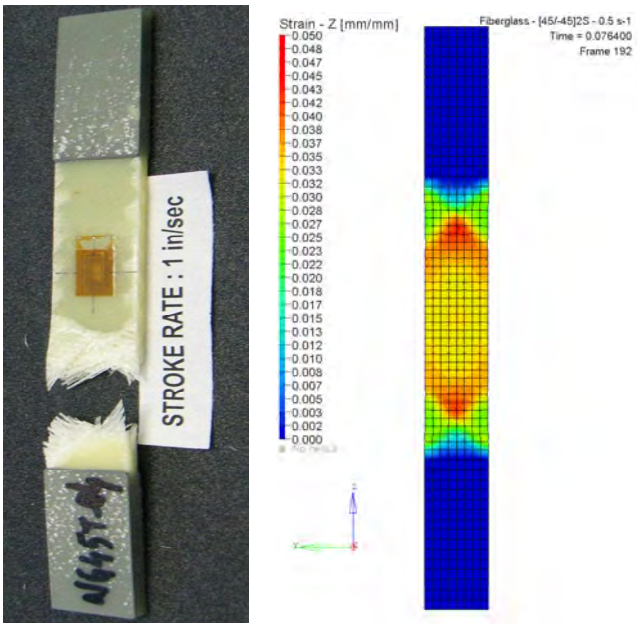

Figure 32. Strain distribution - $[45/-45]_{2S}$ strain-rate of 0.5 s^{-1}.

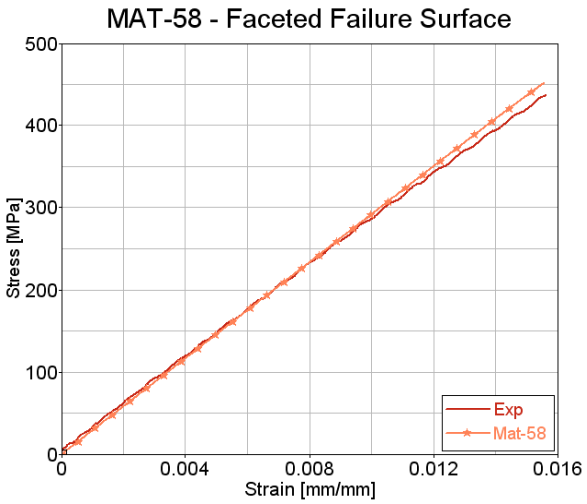

Figure 33. Composite specimen validation for in-plane compression - $[0/90]_{3S}$ strain-rate of 0.0004 s^{-1}.

The model for compression testing is validated with published compressive experimental data for Newport E-Glass fabric 7781/NB321 with stacking sequence $[0/90]_{3S}$ tested at quasi-static strain-rate[7]. The material model implements Ls-Dyna

material card MAT-58. Figure 33 shows good correlation of stress-strain response until failure between experimental and simulation results.

5. CONCLUSIONS AND FUTURE WORK

The following tasks were completed this year:

- Release CBA Phase I report (.," Dynamic Seat Certification by Analysis: Volume I – Hybrid II and FAA Hybrid III ATD Dynamic Evaluation Test Series for SAE ARP 5765") and SAE ARP 5765.
- Development and validation of a component level test for seatbelt webbing material characterization.
- Development and validation of a component level test for seat cushion material characterization.
- The variability in tensile high speed experimental data of Aluminum 7075-T6 and laminated composite materials were evaluated. Limitations of the testing technique and sources of variability were identified.
- A material model for simulation of tensile testing of Aluminum 7075-T6 specimens implementing Ls-Dyna material card MAT-24 along with experimental data from quasi-static strain-rates to 133 s^{-1} was evaluated as a benchmark for high speed tensile testing simulation.
- The effect of shell element formulations, different shell element number of integration points, and two element types were evaluated.
- A numerical model of the specimen-gripping assembly for a high speed servo-hydraulic testing system is assembled and validated with experimental

data at low to medium strain rates. This model will be used in the future to improve the design and test procedures required for high strain rate material data collection.

- A material model for simulation of laminated composites was evaluated for tensile testing implementing Ls-Dyna material cards MAT-54 and MAT-58. A meso-scaled level analysis approach in which lamina properties, thickness, and orientation are introduced is followed. Newport E-Glass fabric 7781/NB321 tensile experimental data generated from quasi-static strain-rates to 5 s^{-1} for different stacking sequences $[0]_4$, $[15/-15]_{2S}$, $[30/-30]_{2S}$, and $[45/-45]_{2S}$ were used for validation.
- A material model for simulation of laminated composites was evaluated for compressive testing implementing Ls-Dyna material card MAT-58. Newport E-Glass fabric 7781/NB321 quasi-static compressive experimental data for stacking sequence $[0/90]_{3S}$ was used for validation.
- Ls-Dyna Material card MAT-58 approximate closely the material response of Newport E-Glass fabric 7781/NB321. Damage parameters should be evaluated to fully understand the development of the different failure modes.

The flowchart shown in figure 34 summarizes the tasks required to develop a methodology to conduct certification by analysis of aircraft composite structures. According to the level of funding provided by the FAA and industry partners, research activities will be defined for FY11 following the roadmap presented in figure 34.

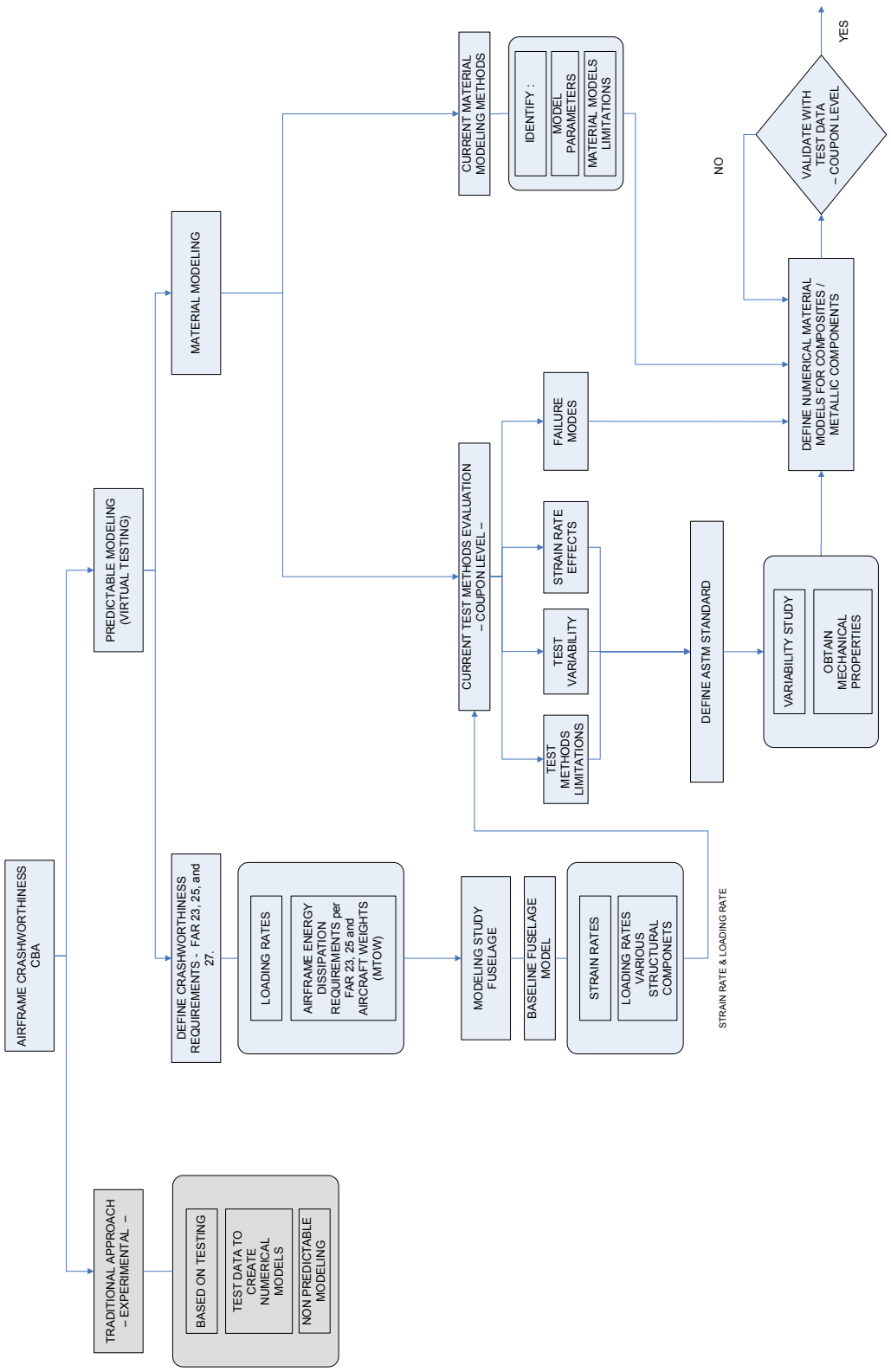

Figure 34. Composite structures crashworthiness.

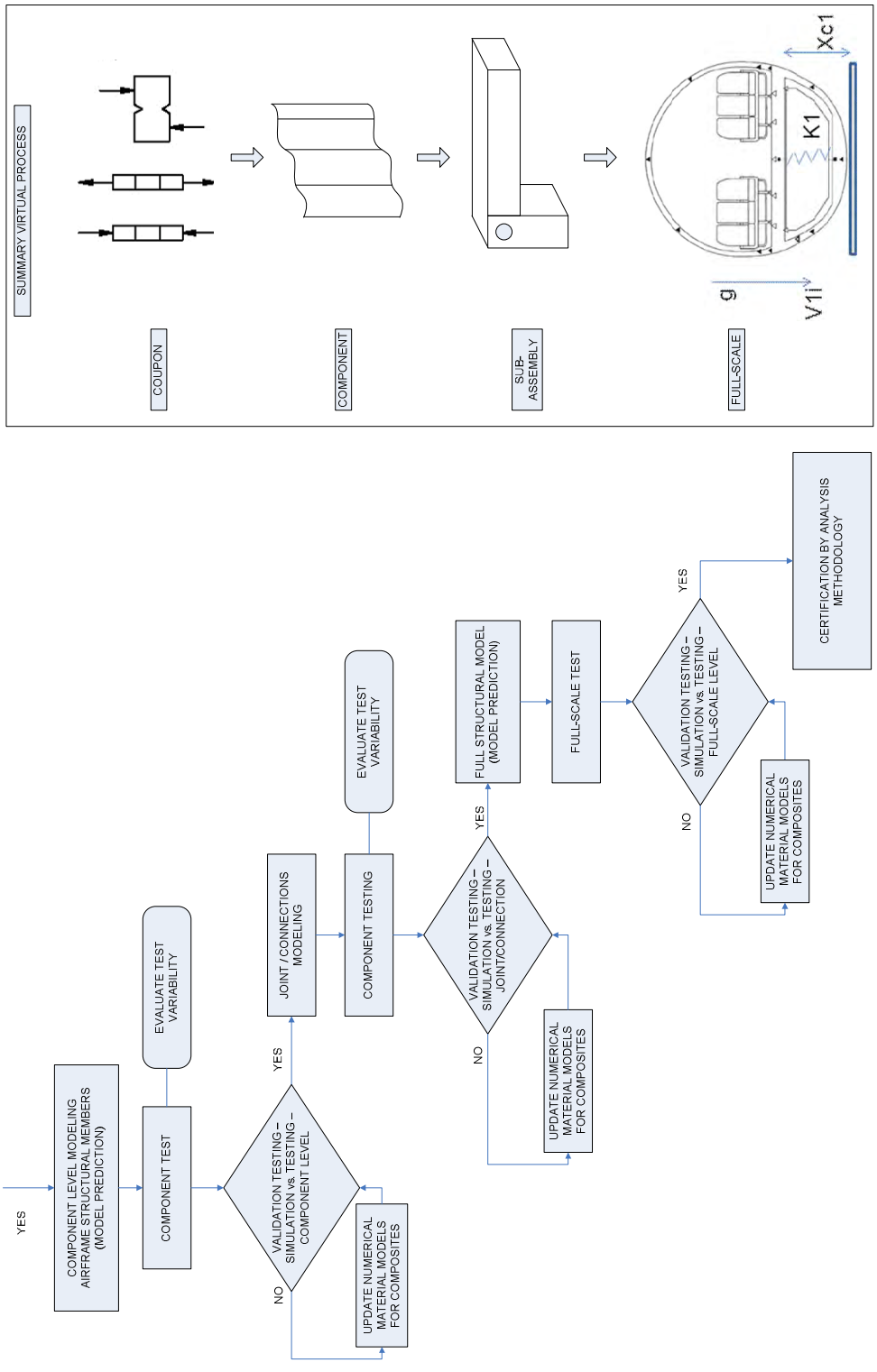

Figure 34. Composite structures crashworthiness (cont.).

REFERENCES

1. Part 23, “Airworthiness Standards: Normal, Utility, Acrobatic, and Commuter Category Airplanes,” *Federal Aviation Administration*, Electronic Code of Federal Regulations (e-CFR), (2009).

2. Part 25, “Airworthiness Standards: Transport Category Airplanes,” *Federal Aviation Administration*, Electronic Code of Federal Regulations (e-CFR), (2009).

3. Hooper, S.J. and Henderson, M.J., “Development and Validation of an Aircraft Seat Cushion Component Test—Volume I ,” DOT/FAA/AR-05/5,I (March 2005)

4. ASTM D-3574-05, “Standard Test Methods for Flexible Cellular Materials—Slab, Bonded, and Molded Urethane Foams,” ASTM International, 100 Barr Harbor Drive, PO Box C700, West Conshohocken, PA 19428-2959.

5. ASTM D3039, “Standard Test Method for Tensile Properties of Polymer Matrix Composite Materials,” ASTM International, 100 Barr Harbor Drive, PO Box C700, West Conshohocken, PA 19428-2959.

6. Raju, K. S. and Acosta, J. F., “Crashworthiness of Composite Fuselage Structures – Material Dynamic Properties (Phase-I),” DOT/FAA/(AR)-XX/XX.

7. LS-DYNA Keyword User’s Manual Version 971, Livermore Software Technology Corporation, Livermore, CA, (2007).

8. Barbero, E., “Finite Element Analysis of Composite Materials,” CRC Press, Boca Raton, (2008).

9. Zheng, X., “Nonlinear Strain Rate Dependent Composite Model for Explicit Finite Element Analysis,” Ph.D. Dissertation, The University of Akron, (2006).

10. Olivares, G.," Dynamic Seat Certification by Analysis: Volume I – Hybrid II and FAA Hybrid III ATD Dynamic Evaluation Test Series for SAE ARP 5765", DOT/FAA/**TBD**, (March 2010)